The Mechanism of Ras GTPase Activation by Neurofibromin†

Robert A. Phillips, Jackie L. Hunter, John F. Eccleston, and Martin R. Webb*

National Institute for Medical Research, Mill Hill, London NW7 1AA, United Kingdom

Received December 6, 2002; Revised Manuscript Received February 11, 2003

ABSTRACT: Individual rate constants have been determined for each step of the Ras·GTP hydrolysis mechanism, activated by neurofibromin. Fluorescence intensity and anisotropy stopped-flow measurements used the fluorescent GTP analogue, mantGTP (2′(3′)-*O*-(*N*-methylanthraniloyl)GTP), to determine rate constants for binding and release of neurofibromin. Quenched flow measurements provided the kinetics of the hydrolytic cleavage step. The fluorescent phosphate sensor, MDCC-PBP was used to measure phosphate release kinetics. Phosphate−water oxygen exchange, using ^{18}O-substituted GTP and inorganic phosphate (P_i), was used to determine the extent of reversal of the hydrolysis step and of P_i binding. The data show that neurofibromin and P_i dissociate from the NF1·Ras·GDP·P_i complex with identical kinetics, which are 3-fold slower than the preceding cleavage step. A model is presented in which the P_i release is associated with the change of Ras from "GTP" to "GDP" conformation. In this model, the conformation change on P_i release causes the large change in affinity of neurofibromin, which then dissociates rapidly.

Small G proteins act as molecular switches within cells, particularly as part of signaling pathways. They have a tightly bound guanine nucleotide, with a significant conformational difference depending on whether GTP or GDP is bound (*1*−*3*). This difference in conformational state determines the activity of the protein with respect to interaction with effectors. When bound to GDP, small G proteins are inactive, but binding to GTP allows it interact with downstream effectors. Several families of small G proteins have been identified, with the first and most studied being the Ras family. The Ras proteins themselves are ∼21 kDa and have a regulatory role in essential functions related to cell growth and differentiation. There are three main mammalian Ras proteins, N-Ras, Kirsten Ras, and Harvey Ras. These are apparently present in all cells, localized to the plasma membrane after post-translational modification adds lipids to the C-terminal region.

The active state of small G proteins and therefore the control of downstream processes are regulated in vivo by two types of protein. Exchange factors (GEFs)[1] catalyze the exchange of the tightly bound GDP for GTP and hence cause activation. Small G proteins have a slow basal GTPase activity, but this is accelerated up to 10^5-fold by GTPase activating proteins (GAPs), thereby inactivating the small G protein (*4*).

A number of GAPs that act on Ras have been isolated, including p120GAP (*5*, *6*) and neurofibromin from mammals (*7*), as well as related proteins from *Drosophila* and yeast. These share sequence motifs that define a GAP-related domain, but most have other domains that are probably involved in controlling the GAP activity. For example, in addition to the catalytic domain, p120GAP has domains that are thought to interact with other signaling molecules. Examples are SH2, SH3, Pleckstrin homology domains, and calcium-dependent phospholipid binding domain. Neurofibromin, on the other hand, does not appear to have well-defined functional domains and may be solely a negative regulator. Crystal structures of a GAP complexed with Ras showed that conserved arginines, in what is now called an arginine finger motif, are intimately located in the Ras catalytic site (*8*, *9*). One arginine takes part in the catalytic process, helping generate a nucleophilic water oxygen to attack the terminal phosphate as well as interacting with the phosphates. It is also apparent that the interaction of this arginine finger stabilizes the effector loop of Ras.

In this current study, we investigate neurofibromin (NF1), which has a 360 amino acid domain that catalyzes GTPase activity in Ras and is homologous to the catalytic domain found in other GAPs (*10*). A major difference from p120GAP, in terms of biochemistry, is that NF1 binds more than 10-fold tighter to Ras·GTP, making maximum activation more attainable experimentally. Here, we use the C-terminal fragment of NF1, containing the complete domain that interacts with Ras.

This work investigates the cleavage step of Ras-bound GTP and subsequent dissociation of the NF1·Ras·GDP·P_i complex, by determining the rate constants for elementary processes in the mechanism. An aim is to understand how structural changes are involved in the GTPase cycle. A working scheme for the NF1-catalyzed hydrolysis of Ras-bound GTP is shown in Scheme 1. The scheme does not include conformation changes as separate processes, although there is a significant change between the Ras·GTP and Ras·GDP structure, as shown in the crystal structures (*3*, *11*, *12*) and exhibited in the differing affinities of the GDP and

† This work was supported by the Medical Research Council, U.K.

* To whom correspondence should be addressed. Tel: (44) 20 8816 2078. Fax: (44) 20 8906 4477. E-mail: mwebb@nimr.mrc.ac.uk.

[1] Abbreviations: GAP, GTPase activating protein; GEF, GTPase exchange factor; NF1, the C-terminal domain of neurofibromin; MDCC-PBP, A197C mutant of phosphate binding protein from *E. coli* labeled with *N*-[2-(1-maleimidyl)ethyl]-7-(diethylamino)coumarin-3-carboxamide; mantGTP, 2′(3′)-*O*-(*N*-methylanthraniloyl)GTP; SH, src homology domain; GMPPNP, guanosine 5′-($\beta\gamma$-imido)triphosphate; DTT, dithiothreitol.

10.1021/bi027316z CCC: $25.00
Published on Web 03/14/2003

Scheme 1

GTP state for NF1 (*13*, *14*). In this scheme, the forward and reverse rate constants and equilibrium constant for any step *i* are given by k_{+i}, k_{-i}, and K_i, respectively.

Step 1 describes the initial binding of NF1 to Ras·GTP. This is followed by the hydrolysis itself, the cleavage of the terminal phosphate from the GTP. In this scheme, P_i release is shown as occurring before dissociation of the NF1·Ras complex, and the data presented here are analyzed in terms of this model. However, the order of release is not established at this stage, and this point is discussed along with alternative mechanisms in the Discussion. In practice, the order of release is probably related to the stage in the mechanism at which the conformation goes from "GTP-like", to which NF1 binds tightly, to "GDP-like", which binds NF1 weakly.

Previous work on the kinetic mechanism has looked at several processes in this mechanism. Eccleston et al. (*15*) and Ahmadian et al. (*16*) both used fluorescent mant nucleotides to examine the rate of NF1 binding. This binding is accompanied by a rapid increase in mant fluorescence. A subsequent, slow fluorescence change could not be assigned unequivocally to a particular process but was assumed to be associated with the hydrolysis step. The rate of P_i release was measured independently and shown to be very similar to the slow phase of the mant fluorescence transient (*17*). The effect of arginine mutations on these fluorescence changes was also determined (*18*). There is little effect on binding due to these mutations but a very large effect on subsequent steps. Time-resolved FTIR studies suggested that P_i release is rate limiting, at least for the low-temperature conditions used (*19*). The work here extends these measurements by using anisotropy to obtain a more direct measure of complex formation and breakdown, and quenched-flow to measure the cleavage rate directly.

Phosphate−water oxygen exchange measurements are used to assess the reversibility of the protein-bound hydrolysis step and subsequent release of P_i. Such measurements have been applied to a variety of ATPases and GTPases, to obtain rates of elementary steps and to elucidate the chemical mechanism of the enzymes (*20*−*24*). This is especially useful in systems such as the actomyosin or mitochondrial ATPases in which the protein-bound hydrolysis step is highly reversible. Two types of oxygen exchange reactions are used here and are shown in Figure 1.

Intermediate exchange measurements use (γ-$^{18}O_3$)GTP, in which the three nonbridging oxygens of the terminal phosphate are substituted with close to 100% of the stable isotope ^{18}O. During hydrolysis by Ras and NF1, the isotope exchanges with water oxygens: i.e., ^{18}O is lost from the phosphate to water. The extent of this exchange is measured by comparison of the isotopic enrichment in the substrate GTP and the product P_i. During the hydrolysis step, ($^{18}O_3$)P_i is formed together with unlabeled GDP, initially as the protein-bound GDP·P_i state (Figure 1a). Apart from the possibility of small isotope effects, the ^{18}O and ^{16}O are the same chemically and biochemically. Previous work on other systems suggests that the tetrahedral P_i can rotate freely in the binding site so that all four oxygens are essentially equivalent (*20*). The GDP·P_i state can then undergo two fates. First, the P_i can be released from the catalytic site as ($^{18}O_3$)P_i, that has undergone no exchange. Because of the weak binding of P_i to the protein, as elucidated later in this work, this released P_i takes no further part on the time scale used for the intermediate exchange measurement.

Second, apart from releasing P_i, the protein-bound GDP·P_i complex can re-form bound GTP, with loss of one oxygen atom from P_i as water is formed. Because of the free rotation of P_i, one-quarter of the time, a ^{16}O is lost and the initial (γ-$^{18}O_3$)GTP is re-formed; three-quarters of the time, an ^{18}O is lost and (γ-$^{18}O_2$)GTP is formed. In both cases, this GTP must eventually be hydrolyzed. Further reversals of the hydrolysis step can in principle lead to a mixture of ($^{18}O_3$)P_i, ($^{18}O_2$)P_i, ($^{18}O_1$)P_i and unlabeled P_i, released from the protein. The product P_i is isolated and the distribution of isotope is determined by mass spectrometry. The extent of exchange depends on the partitioning of the GDP·P_i complex between GTP re-formation and P_i release and, so, depends on the ratio of k_{-2} and k_{+3}. The quantitative treatment of these data, as well as the main analytical procedures by mass spectrometry to obtain the proportions of different ^{18}O-labeled P_i species, has been described (*20*, *25*). Here we can obtain a separate assessment of k_{+3} by direct measurement of P_i release kinetics, so that the intermediate oxygen exchange data can be used to assess k_{-2}.

In medium exchange measurements, ($^{18}O_4$)P_i in the medium is incubated with the protein-bound GDP complex. If some of this P_i binds, then the GDP·P_i complex is formed, and this can partition between the two processes as described above, namely, forming (γ-$^{18}O_3$)GTP with loss of one ^{18}O to water, or simple release of ($^{18}O_4$)P_i with ^{18}O unaltered (Figure 1b). The extent of exchange to the ($^{18}O_4$)P_i once bound depends on k_{+3}/k_{-2} as above. But the extent of exchange to the ($^{18}O_4$)P_i in the medium also depends on the rate of binding of this P_i to the GDP complex (k_{-3}), and so

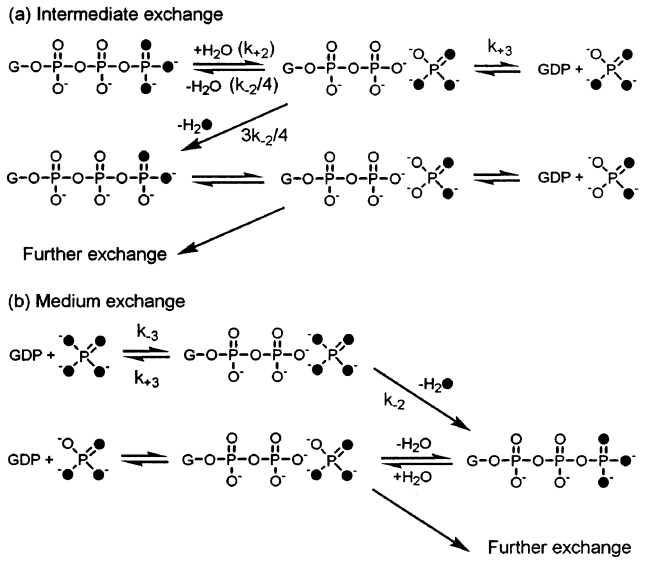

FIGURE 1: Reaction schemes, showing the mechanism of oxygen exchange. Oxygen-18 is shown by filled Os.

this measurement allows assessment of k_{-3}, given the values already obtained for k_{-2} and k_{+3}. The quantitative treatment of medium exchange data has been described previously (*26*, *27*).

Much of the work here uses mantGTP to provide fluorescence signals for determination of rate constants. Previous work suggests that the ribose modification to obtain this analogue has only minor effects on the interactions of nucleotide with Ras and the complex with NF1. Generally for small G proteins, rates and equilibrium constants with mant nucleotides are within 2-fold of those found with the natural nucleotide (*15*, *28*). The structure of Ras with a mant-nucleotide bound is almost identical to that with the natural nucleotide (*29*). Essentially the mant is on the surface of the protein, as the ribose oxygens are exposed from the binding site in both GDP and GTP complexes. There are some direct comparisons available for GAPs with mantGTP and GTP. The k_{cat} values for GTPase activation by p120-GAP are similar with Ras·mantGTP and Ras·GTP, although the K_m is 2-fold smaller with the analogue (*17*). A measurement of the overall GTPase activity at saturating NF1 showed that the k_{cat} values are within 10% of each other for Ras·mantGTP and Ras·GTP. Specifically the P_i release rate is 25% higher for Ras·GTP than that for Ras·mantGTP. Thus, we consider it unlikely that the presence of the mant fluorophore significantly affects the NF1-activated mechanism.

EXPERIMENTAL PROCEDURES

Materials. N-Ras and Ha-Ras (Q61L) (residues 1−166) were prepared using an *Escherichia coli* expression system (*30*, *31*). Except as indicated, "Ras" in this work refers to wild-type N-Ras, which is isolated as the GDP complex. Because it has very slow intrinsic GTPase activity, Ha-Ras (Q61L) was purified as its GTP complex. A neurofibromin fragment containing the GAP-related domain and comprising residues 1195−1528 (*32*) was prepared using an *E. coli* expression system (*15*). This fragment is referred to as NF1 in this work. The P_i sensor, MDCC-PBP was prepared as described (*33*). Proteins and protein−nucleotide complexes were stored at −80 °C.

$(^{18}O_4)P_i$ and $(\gamma\text{-}^{18}O_3)$GTP were synthesized from (^{18}O)water (97% enriched) as described (*20*). MantGTP, mantGDP, and mantGMPPNP were synthesized and purified using described methods (*34*, *35*). Complexes of Ras·mantGTP, Ras·mantGDP, and Ras·$(\gamma\text{-}^{18}O_3)$GTP were formed as described by Newcombe et al. (*36*). Ras·GMPPNP and Ras·mantGMPPNP complexes were prepared as described by Hirshberg et al. (*37*) and analyzed by HPLC using a Whatman Partisphere SAX column (12.5 × 0.45 cm) in a mobile phase (at 1.5 mL min^{-1}) of 75% (v/v) 0.5 M $(NH_4)_2HPO_4$, adjusted to pH 4.0 with concentrated HCl, with 25% methanol. Typically, mantGTP complexes were 95% triphosphate.

All kinetic measurements were done in 20 mM Tris·HCl, pH 7.6, 1 mM $MgCl_2$ at 30 °C.

^{18}O Exchange Measurements. Medium exchange experiments were performed by incubating 0.5 mM $(^{18}O_4)KH_2PO_4$ solution with 10 μM Ras·mantGDP and 10 μM NF1 in 20 mM Tris·HCl, pH 7.6, 1 mM $MgCl_2$ at 30 °C. Incubations were carried out for 7 and 24 h. Control measurements were obtained for incubations containing no protein, NF1 only, and Ras·mantGDP only.

Intermediate exchange measurements were performed by mixing 100 μM Ras·$(\gamma\text{-}^{18}O_3)$GTP with 10 μM NF1 for 30 s using the solution conditions above. The enrichment of the starting $(\gamma\text{-}^{18}O_3)$GTP was determined by transferring the terminal phosphate first to ADP, using nucleosidediphosphate kinase, and then hydrolyzing the resulting ATP in a reaction known to produce no exchange, to give $(^{18}O_3)P_i$ (*38*).

P_i was analyzed for distribution of different ^{18}O-labeled species as described previously (*25*), but with the following modifications. All solutions were made with deionized, distilled water. The P_i was purified on Q-Sepharose (250 μL), prewashed with 3 mM HCl (5 mL; Aristar, VWR International), water (5 mL), then 5 mM Tris·HCl, pH 7.5 (2.5 mL; made using Aristar Tris, VWR International). The columns were not reused. The P_i samples were loaded as diluted solutions, and the column was washed with water (500 μL), then 1 mM HCl (2 mL). The P_i was eluted with 3 mM HCl (3 mL). P_i from $(\gamma\text{-}^{18}O_3)$GTP hydrolysis was detected by addition of trace $[^{32}P]P_i$ prior to loading the column. P_i from the medium $(^{18}O_4)P_i$ incubation was detected using the phosphate sensor, MDCC-PBP (*33*). Aliquots of the eluate (1 μL) were added to 1 μM MDCC-PBP in 10 mM PIPES pH 7.0 (200 μL) and the change in fluorescence measured (excitation 430 nm, emission 465 nm). The other change from the published procedure was that analyses were performed using a Hewlett-Packard gas chromatograph model 5890, equipped with a mass selective detector model 5971.

Data were corrected for the starting enrichment as described (*25*, *39*). For the exchange using $(\gamma\text{-}^{18}O_3)$GTP (Figure 1a), the equations have been defined elsewhere for the proportions of different ^{18}O-labeled P_i species as a function of the ratio of rate constants, k_{+3}/k_{-2} (*25*). The best-fit values for this ratio were determined using an iterative procedure. For the medium exchange measurements, the starting enrichment was calculated from the ^{18}O-distribution determined from the control incubation in the absence of protein. In practice, there was almost no exchange in this control, and so this distribution was extremely close to that from analysis of the starting $(^{18}O_4)P_i$. The data were fitted to a simulation of the time course of the scheme in Figure 1b using Scientist software (Micromath, St Louis, MO) to obtain global best fits for the rate of exchange.

Other Measurements. Stopped flow experiments were carried out in a HiTech SF61MX apparatus with a mercury−xenon light source and HiTech IS-2 software. For MDCC-PBP fluorescence, the excitation wavelength used was 436 nm, and a 455 nm cutoff filter (Schott glass) was used to collect emitted light. For mant, 366 nm was used to excite, and a 400 nm cutoff filter (Schott glass) was used to collect light. Anisotropy was measured with the instrument in the "T" format, allowing simultaneous acquisition of horizontal ($I_{||}$) and perpendicular ($I_{\perp}$) components. This enabled anisotropy, $(I_{||} - I_{\perp})/(I_{||} + 2I_{\perp})$, and intensity $(I_{||} + 2I_{\perp})$ to be calculated from the same reaction profile (*40*). In experiments described, the quoted concentrations are those in the mixing chamber except where stated. Data were fitted to theoretical curves using the HiTech software or Grafit (*41*) and are presented here as averages of 2−4 individual traces.

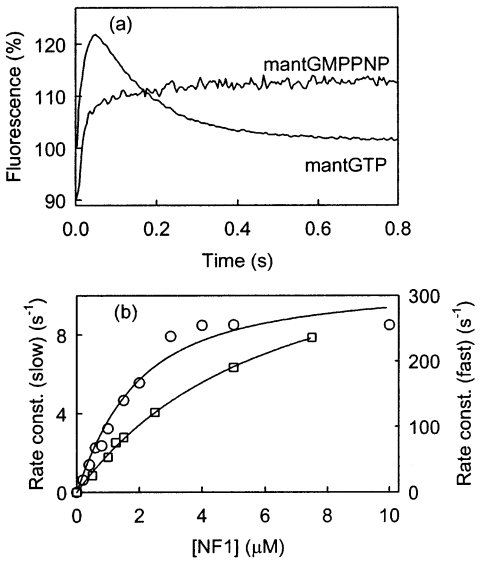

FIGURE 2: Fluorescence intensity changes following mixing Ras·mantGTP with excess NF1. (a) The profile obtained when 1 μM Ras·mantGTP or Ras·mantGMPPNP was mixed with 10 μM NF1. The reaction conditions are described in the text. The curve for mantGTP was fitted to a double exponential. The trace for mantGMPPNP is offset by 10% for clarity. (b) Dependence on NF1 concentration of the rate constants of the two phases. Circles are the slow phase, squares the fast phase. The best-fit hyperbolas are shown.

Quenched flow measurements were carried out in a HiTech apparatus using different length loops and flow rates to age reactions before quenching. Reactions (in a total volume of 300 μL) were quenched using 10% perchloric acid (150 μL) and then partially neutralized to pH ~4 using 4 M sodium acetate (50 μL). Samples were then analyzed by HPLC using a Whatman SAX-10 Partisil column (0.4 × 25 cm) at 1.5 mL min^{-1} in a mobile phase of 75% (v/v) 0.5 M $(NH_4)_2HPO_4$, adjusted to pH 4.0 by HCl, and 25% methanol. Mant fluorescence was monitored on a Hitachi F-1050 fluorescence spectrophotometer, connected to the HPLC column, using an excitation wavelength of 366 nm and detecting emission at 440 nm. Peaks for mantGDP and mantGTP were integrated using a Hewlett-Packard 3390A integrator.

Steady-state fluorescence was measured using a Perkin-Elmer LS50B fluorometer with a xenon light source. Absorbance spectroscopy was carried out using a Beckman DU640 spectrophotometer. Anisotropy titrations were carried out using an ISS PC1 photon counting spectrofluorimeter in the "T" format, exciting the mant fluorophore at 366 nm and using a 400 nm cutoff (Schott glass) filter.

RESULTS

The Effect of NF1 on Mant Fluorescence: Binding Kinetics. When Ras·mantGTP was mixed with NF1, a biphasic trace was observed over the time course of the fluorescence intensity (Figure 2a). An initial fast increase was followed by a slower decrease. The first phase has been interpreted as due to NF1 binding to Ras·mantGTP (step 1 in Scheme 1) (*15*). The second phase is due to either subsequent mantGTP hydrolysis or dissociation of the NF1·Ras·GDP·P_i complex, i.e., a step in the mechanism of Scheme 1 after NF1·Ras·GTP formation. At 10 μM NF1 and 1 μM Ras·GTP, the biphasic trace (Figure 2a) shows a large, very rapid initial increase in intensity (236 s^{-1}) followed by a slower large decrease (8.3 s^{-1}). The starting and final fluorescence intensities are identical in this time course, as expected because the species are Ras·mantGTP and Ras·mantGDP, which have similar fluorescence intensities when not complexed with another protein (*28*).

Scheme 2

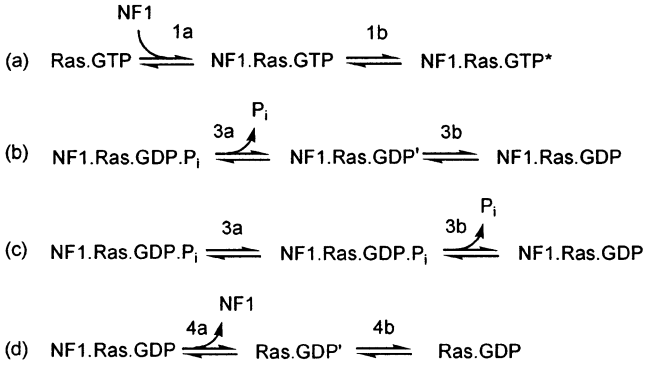

The rate constant for association (step 1) has been determined previously over a range of NF1 concentrations using mant fluorescence (*16*). Under the conditions used here, the rate of the fast rise also has a hyperbolic dependence on NF1 concentration (Figure 2b). This suggests that the binding is in fact two steps (Scheme 2a), bimolecular binding per se followed by a conformation change. The latter is accompanied by the fluorescence change and is rate limiting at high NF1 concentration. The best-fit hyperbola gave $1/K_{1a}$ as 5.4 μM and $k_{+1b} + k_{-1b}$ as 418 s^{-1}, assuming that step 1a is rapid and reversible.

The slow phase of mant fluorescence on mixing NF1 with Ras·mantGTP also has an approximately hyperbolic dependence on NF1 concentration. Analysis in terms of two consecutive processes (1′ and 2′) gives a hyperbolic best fit of $1/K_{1'}$ as 1.3 μM and $k_{+2'} + k_{-2'}$ as 10.7 s^{-1}. The meaning of this analysis is described in the discussion.

Various measurements were done to determine the rate constants for other specific processes described by the mechanism in Scheme 1. They were performed at 10 μM NF1 and 1 μM Ras unless otherwise stated. Figure 2b indicates that the choice of these concentrations ensure close to saturation of binding, and so errors are minimized due to slight variations in activity and concentration of different protein preparations. The measurements are presented in the order as they relate to forward steps in the sequence shown in Scheme 1. Oxygen exchange measurements are then described that monitor reverse steps in this Scheme.

Kinetics of NF1 Binding to Ras·mantGTP. Two types of measurements were used to clarify the interpretation of the two phases in Figure 2a.

On mixing Ras·mantGMPPNP with saturating NF1, the time course for mant fluorescence intensity shows a single rapid phase, similar to the rapid phase with mantGTP but not the slow second phase (Figure 2a). This is consistent with the rapid phase being due to binding of NF1, but no slow phase occurs since there is no hydrolysis of mantGMPPNP. Similar results were obtained using the Q61L mutant of Ras that has very slow hydrolysis with NF1, insignificant over the time course of the binding measurement (data not shown).

Fluorescence anisotropy measured on mixing NF1 with Ras·mantGTP showed a similar reaction profile to mant

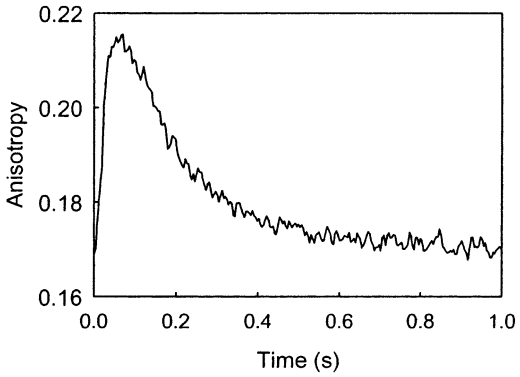

FIGURE 3: The anisotropy time course following mixing 1 μM Ras·mantGTP with 10 μM NF1. The data were fitted to a double exponential to obtain rate constants for binding (fast phase, 185 s^{-1}) and dissociation (slow phase, 7.5 s^{-1}) of NF1 and Ras. See text for details.

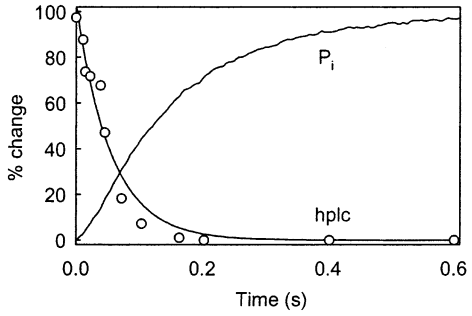

FIGURE 4: MantGTP cleavage and subsequent P_i release during NF1-mediated hydrolysis of Ras·mantGTP. The cleavage of mantGTP (circles) was measured by quenched flow and analyzed for mantGTP and mantGDP content by HPLC. In the quenched-flow measurement, 1 μM Ras·mantGTP was rapidly mixed with 10 μM NF1, and the reaction was quenched at defined times with acid as described in the Experimental Procedures. HPLC analysis was used to determine the percentage of mantGDP formed at each time point. The line is the best fit exponential. P_i release was measured by MDCC-PBP fluorescence, using 5 μM of the P_i sensor. The latter is shown as percent change of the maximum signal in order to get both sets of data on the same scale.

fluorescence intensity (Figure 3). Anisotropy is dependent on the rate of rotational tumbling of the fluorophore, in turn related to the size of the complex assuming there is little local motion. So the size of anisotropy can be related more directly to NF1 association to and dissociation from Ras·mantGTP. Anisotropy data for Ras·mantGMPPNP and Q61L Ras·GTP showed a similar kinetics to intensity, i.e., a single fast phase (data not shown). These experiments are consistent with previous conclusions: binding of NF1 to Ras in the triphosphate state occurring in two steps, association itself followed by a conformation change. In the case of NF1·Ras·mantGTP, the fluorescence trace then shows a slow decrease.

Kinetics of the Hydrolysis Step. Quenched-flow measurements were performed to determine the rate of the hydrolytic cleavage step (step 2 from Scheme 1). The extent of conversion of protein-bound mantGTP to protein-bound mantGDP was measured at individual time points, by HPLC analysis of acid-quenched reaction mixture (Figure 4). The data gave a best fit of 19.5 s^{-1} for the cleavage rate.

Kinetics of P_i Release. P_i release during mantGTP hydrolysis was measured using the fluorescent phosphate sensor, MDCC-PBP (*42*). On mixing Ras·mantGTP with

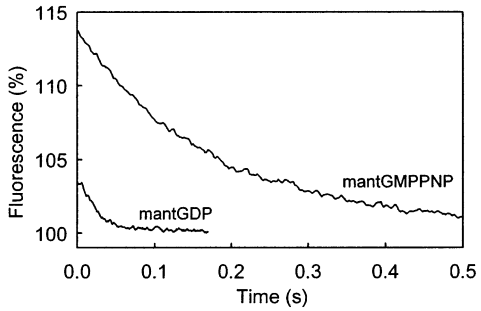

FIGURE 5: Dissociation of NF1 from Ras·mantGMPPNP and Ras·mantGDP. The fluorescence intensity was followed after mixing preformed NF1·Ras·mantGMPPNP or NF1·Ras·mantGDP with a trap of excess Ras in a non-hydrolyzable triphosphate form. The preformed complex was made by mixing 2 μM NF1 and 2 μM Ras·mantGMPPNP (syringe concentrations). The trapping Ras was 10 μM Ras·GMPPNP (mixing chamber concentration). For the diphosphate, high concentrations were required to obtain a signal due to weak NF1 binding. 40 μM NF1 and 20 μM Ras·mantGDP (syringe concentrations) were mixed, and the trapping Ras was 200 μM Q61L Ras·GTP (mixing chamber concentration).

NF1, there was a lag phase, followed by an increase in fluorescence intensity with a rate of 7.8 s^{-1} (Figure 4). The lag phase is approximately the size expected for binding and cleavage (steps 1 and 2) to occur. The sensor then gives a direct measure of subsequent dissociation of P_i from the complex, showing that this is approximately 3-fold slower than the cleavage step.

Kinetics of NF1 Dissociation. When NF1 was mixed with Ras·mantGTP, the slow phase of mant fluorescence intensity and anisotropy (Figures 2 and 3) had similar kinetics. The anisotropy probably represents the dissociation of NF1 from Ras·mantGDP, as rationalized above, hence suggesting that the intensity change also monitors this step. However, this rate constant (7.5 s^{-1}) is similar to that of P_i release (7.8 s^{-1}), so the P_i and NF1 dissociate concomitantly. It is not possible to determine directly if these two dissociations are truly simultaneous or whether there is ordered dissociation. In the latter case, the first species would be released with slow kinetics, and this rate then would determine the observed kinetics of the second dissociation. We discuss this point later.

To measure the rate constant of NF1 dissociation for Ras·mantGDP (step 4) directly, preformed NF1·Ras·mantGDP was mixed into a large excess of Q61L Ha-Ras·GTP, and the fluorescence followed with time (Figure 5). This Ras mutant hydrolyzes GTP very slowly with an intrinsic rate of 1.0×10^{-5} s^{-1}, which is accelerated only 6-fold in the presence of saturating NF1 (*14*). The Ha-Ras·GTP forms a tight complex with NF1 with a K_d of 0.1 μM and so traps NF1 as it dissociates from the Ras·mantGDP complex, preventing reassociation with Ras·mantGDP. The fluorescence decrease monitors the dissociation of NF1·Ras·mantGDP. The rate was 46 s^{-1}, severalfold faster than that measured in a single turnover starting from NF1·Ras·mantGTP (Figure 2). Note that it was not feasible to increase the protein concentrations significantly in order to check that the dissociation was cleanly rate limiting in this "chase" measurement. However, according to assessment of the likely rate constant for Ras·GTP binding to NF1 under the conditions used, this is at least 5-fold faster than the measured rate, hence validating that the measured rate was due to dissociation.

Table 1: Distribution of Oxygens in P_i from (γ-$^{18}O_3$)GTP Hydrolysis[a]

	^{18}O per P_i (%)				best fit
	0	1	2	3	k_{+3}/k_{-2}
expt 1	0	1.4	1.5	97.1	
best fit	0	0	2.2	97.8	33.1
expt 2	0	1.4	1.2	97.4	
best fit	0	0	1.9	98.1	39.1

[a] Data are corrected for the enrichment of ^{18}O in the starting GTP (92.5%) to give what would be for 100%. The best fits are determined as described (*25*, *39*).

Kinetics of NF1 Dissociation from a Triphosphate Complex of Ras. In addition to all the forward rate constants of Scheme 1, most of the reverse rate constants were also measured, at least to give approximate values. It is not possible to measure the dissociation rate with GTP complexes and wild-type proteins because of the rapid hydrolysis. Dissociation of NF1 from Ras·mantGMPPNP was determined by mixing preformed NF1·Ras·mantGMPPNP with a large excess of Ras·GMPPNP to prevent reassociation with Ras·mantGMPPNP (Figure 5). The observed rate, limited by dissociation, was 5.5 s^{-1}.

Kinetics of the Reverse of Phosphate Release and Cleavage. Two types of oxygen isotope exchange measurements were performed to assess the rate constants of the reverse of steps 2 and 3. The rationale for these measurements was described in the Introduction.

When Ras·(γ-$^{18}O_3$)GTP was hydrolyzed in the presence of NF1, the main P_i species formed was ($^{18}O_3$)P_i, showing that there was very little exchange and the P_i release is much faster than GTP re-formation. The data are shown in Table 1, and the best fit gives an average value of 36 for k_{+3}/k_{-2}. k_{+3} was determined as 8 s^{-1} (Figure 4), so k_{-2} as 0.22 s^{-1}. Because of the low extent of exchange, values for this ratio up to 60 are consistent with the data, and so a value of k_{-2} can be estimated only within a factor of 2.

During medium exchange, a slow exchange of oxygen atoms takes place between ($^{18}O_4$)P_i in the medium and water, when incubated with NF1 and Ras·mantGDP. To observe significant exchange required incubations of several hours. However, the proteins appear to remain active for the whole time as incubations for 7 and 24 h showed that exchange occurred at a constant rate over this time period. Table 2 summarizes the results, together with the best-fit simulations, from which is extracted a value for k_{-3} of 108 M^{-1} s^{-1}, as described in Table 2.

Effect of P_i in the Medium on Rate Constants. A single cycle of NF1 interaction with Ras·mantGTP was carried out in the presence of 10 mM phosphate to determine whether high P_i concentration inhibited the NF1 release step, and thereby changed the fluorescence intensity and anisotropy traces. A significant effect of P_i in this measurement would have implications for the mechanism (see Discussion). To ensure that any effect was due to P_i itself, rather than a change in ionic strength due to its presence, a control was also performed using 20 mM KCl instead of P_i. With both KCl and P_i, a similar small change in rate constant was observed to 9.8 (intensity with KCl), 9.0 (anisotropy with KCl), 9.0 (intensity with P_i), and 10.0 s^{-1} (anisotropy with P_i). There was no change in relative amplitudes of the two phases.

Table 2: Distribution of Oxygens in P_i Following Incubation of Medium ($^{18}O_4$)P_i with Ras·mantGDP and NF1[a]

[Ras] (μM)	[NF1] (μM)	time (h)	oxygens exchanged per P_i (%)				rate[b] (h^{-1})
			0	1	2	3	
10	0	24	87.0	11.9	1.0	0.1	
		best fit[c]	*87.1*	*12.2*	*0.7*	*0*	0.0060
0	10	24	95.1	3.8	0.8	0.3	
		best fit[c]	*95.6*	*4.3*	*0.1*	*0*	0.0019
10	10	7	81.9	15.8	2.0	0.3	
		best fit[c]	*82.4*	*16.4*	*1.2*	*0*	0.0278
10	10	24	55.0	33.0	9.8	2.2	
		best fit[c]	*55.5*	*35.1*	*8.5*	*0.9*	0.0247

[a] Data are corrected for the enrichment of ^{18}O in the starting P_i (96.3%) to give what would be for 100%. The percent P_i with four exchanged oxygens could not be assessed accurately, as this P_i is unlabeled and so is indistinguishable from the small amount of contaminant P_i always present in this type of solution. Each distribution is the average of two independent experiments—see note *d*. [b] This rate is defined as $k_{-3}k_{-2}$[NF1·Ras·mantGDP]/($k_{+3} + k_{-2}$). When one protein is omitted, the total protein concentration was used. See note *d*. [c] The best fit was calculated as described in the text. [d] For this measurement, the calculation is described to obtain k_{-3}. The two individual measurements gave distributions 81.3, 16.2, 2.1, 0.4 and 82.5, 15.3, 1.9, 0.3. The best-fit rates were 0.0288 and 0.0268 h^{-1}, respectively. The main species catalyzing exchange is NF1·Ras·mantGDP. To calculate the rate due to this species and correct for the slow exchange due to the individual proteins, the concentration of each protein species must be calculated using the dissociation constant of NF1·Ras·mantGDP at these conditions, 38 μM (*14*). This gives 1.8 μM NF1·Ras·mantGDP, 8.2 μM NF1, and 8.2 μM Ras·mantGDP. Correcting for the exchange due to the individual proteins gives a 0.0215 h^{-1} average rate of exchange due to the complex. So $k_{-3}k_{-2}/(k_{+3} + k_{-2})$ is 0.0120 μ^{-1} h^{-1}. Using the value of $k_{+3}/k_{-2} = 36$ from the data in Table 1, k_{-3} is 123 M^{-1} s^{-1}. A global fit was done to the complete set of data for the time course of exchange, giving a rate of exchange of 0.0252 h^{-1}, and so k_{-3} is 108 M^{-1} s^{-1}.

Effect of P_i on Affinity of NF1 for Ras·mantGDP. Anisotropy measurements were done as described previously during a titration of NF1 into Ras·mantGDP (*14*), but in the presence of 10 mM P_i or 20 mM KCl (data not shown). The K_d values obtained were 48 and 40 μM, respectively, suggesting only a small effect of P_i at most, as the value in the absence of these additions is 38 μM.

High Ionic Strength Conditions. Previous studies have shown that there may be a difference between the rate of mant fluorescence intensity change and P_i release under conditions of high ionic strength (*15*, *17*). However, those measurements were done at different times with different protein preparations. In an attempt to differentiate between P_i release and NF1 dissociation, measurements were made at 100 mM NaCl using the same solutions, with only MDCC-PBP added to the one to measure P_i (data not shown). This ionic strength had been shown previously to give the maximum rates. Although rates increased compared with those at zero NaCl, P_i release at 13.8 s^{-1}, mant intensity change at 15.1 s^{-1}, and anisotropy change at 15.4 s^{-1} do not differ significantly.

DISCUSSION

Rate Constants for a Minimal Reaction Scheme. The kinetic mechanism for the hydrolysis of Ras·GTP by NF1 at 30 °C has been determined mainly using mantGTP to provide fluorescence signals. The values of rate constants are summarized in Table 3. In terms of Scheme 1, rate constants can be put to each step, forward and reverse except

Table 3: Values of Rate and Equilibrium Constants at 30 °C[a]

parameter	value	method
$1/K_{1a}$	5.3 μM	NF1 + Ras·mantGTP fluorescence
k_{+1b}	418 s^{-1}	NF1 + Ras·mantGTP fluorescence
k_{-1b}	5.5 s^{-1}	NF1·Ras·mantGMPPNP fluorescence
k_{+2}	19.5 s^{-1}	quenched flow
k_{-2}	0.22 s^{-1}	intermediate oxygen exchange
k_{+3}	7.8 s^{-1}	P_i sensor
k_{-3}	108 M^{-1} s^{-1}	medium oxygen exchange
k_{+4}	46.5 s^{-1}	NF1·Ras·mantGDP fluorescence
k_{-4}	1.2 μM^{-1} s^{-1}	determined from K_4 (*14*)

[a] The rate constants are as in Schemes 1 and 2.

for k_{-4}. Because of the weak binding of Ras·GDP to NF1, it would be difficult experimentally to get conditions that allow determination of this rate constant. However, a value may be calculated using the value of K_d, equivalent to K_4, as 38 μM, previously reported (*14*), and the value for k_{+4} determined here, 46.5 s^{-1}. This gives k_{-4} as 1.2×10^6 M^{-1} s^{-1}.

As shown in previous work (*16*), NF1 binds to Ras·mantGTP in two steps. The simplest mechanism (Scheme 2) is bimolecular binding followed by a rapid conformation change that is accompanied by the fluorescence change. The intercept with the *y* axis in Figure 2b should give a value of k_{-1b} for Ras·mantGTP. However, the intercept is too close to the origin to obtain an accurate value. A measurement equivalent to k_{-1b} was done with Ras·mantGMPPNP because the measurement would not be possible with the GTP complex due to hydrolysis. This gave a value of 5.5 s^{-1}, which is consistent with the intercept in Figure 2b. The fit in Figure 2b gives 418 s^{-1} as the maximum rate, equivalent to k_{+1b}, as k_{-1b} is very low.

This analysis suggests a conformation change associated with NF1 binding. NF1 binds to Ras in the Switch I region close to the nucleotide (*8*), so the conformation change reported by mant fluorescence may simply be a movement of mant to accommodate the NF1. Also, NF1 inserts an arginine into the catalytic site of Ras to produce the complex, activated for hydrolysis as described in the Introduction. This insertion may be associated with step 1b.

The slow phase of mant fluorescence on mixing NF1 with Ras·mantGTP also has an approximately hyperbolic dependence on NF1 concentration. The rate of this phase is due to P_i release although the fluorescence change is likely to be associated with subsequent rapid NF1 release. Thus, the maximum rate (10.7 s^{-1}) is strictly given by $k_{+3} + k_{-3}[P_i]$. However, $k_{-3b}[P_i]$ is very low, so that this 10.7 s^{-1} is equivalent to k_{+3} and is consistent with that obtained by direct measurement using the P_i sensor (7.8 s^{-1}). The best-fit hyperbola to the data gave $1/K_{1'}$ as 1.3 μM, which is similar to the concentration of Ras used, so this value for $K_{1'}$ is not accurate. In fact, the shape of the curve of slow phase NF1 dependence is dependent on a combination of rate constants for steps 1a, 1b, and 2. Overall, these steps are not rapid and reversible relative to P_i release. Interpretation of $1/K_{1'}$ is therefore of limited use and is not pursued here.

Comparison of the NF1-Stimulated and the Intrinsic Ras GTPase Activity. Ras GAPs accelerate the overall rate of GTP hydrolysis by some 10^5-fold. A set of rate constants has been determined for the intrinsic GTPase activity of N-Ras at 37 °C (*43*). Under these conditions, the cleavage rate is 3.4×10^{-4} s^{-1} and so is likely to be $\sim 1 \times 10^{-4}$ s^{-1} at 30 °C. Oxygen exchange data suggest that the P_i release kinetics are similar to that of the cleavage step (*44*). Thus, both these steps are accelerated by the presence of NF1. The structural rationale for GAP catalysis of the cleavage step itself is described in the Introduction. At present there is no exact structural explanation as to how the NF1 might facilitate P_i leaving the catalytic site.

Order of Dissociation of NF1·Ras·GDP·P_i. The data presented here gives a fairly full kinetic description of the mechanism in Scheme 1. Several questions arise concerning this Scheme and we will deal with these in turn.

As stated in the Introduction, there is no reason a priori to assume that during dissociation of NF1·Ras·GDP·P_i one species in the complex necessarily leaves before another. Our data suggest that the release of P_i (at 7.8 s^{-1}) and dissociation of NF1 (7.5 s^{-1}) have identical observed kinetics and that the observed rate constants remain the same under all conditions studied. It is likely that there is ordered dissociation: one species dissociates first, and the other species cannot dissociate until after the first. So the second dissociation has an observed rate limited by that of the first species. Our data agree with time-resolved FTIR data that suggest P_i release is rate-limiting in the NF1-catalyzed GTPase reaction (*19*). In Scheme 1 and throughout, we assume that P_i release is followed by NF1 dissociation; i.e., P_i release triggers that of NF1. The measurement of NF1 dissociation from Ras·mantGDP as 46.5 s^{-1} is consistent with this, as the rate constant observed for NF1 dissociation from the putative NF1·Ras·mantGDP is severalfold slower. A proviso is discussed below: it is possible that the NF1·Ras·mantGDP complex formed by addition of NF1 to Ras·mantGDP is not the same as that formed via hydrolysis of NF1·Ras·mantGTP.

We must also consider the possibility that NF1 dissociates first and that this triggers P_i release. If this were the case, it would be likely, but not absolutely required, that the presence of P_i in the medium would have an effect on the strength of NF1 binding to Ras·GDP. That was not found to be the case, as shown by the titration of NF1 into Ras·mantGDP in the presence of P_i. Furthermore, this model would suggest that the transition from "GTP-like" to "GDP-like" structure of Ras is associated with cleavage, resulting in weakened NF1 binding. Other evidence suggests that the conformation change may occur associated with P_i release (*45*). So although the dissociation of NF1 before P_i cannot be excluded, it seems less likely than the reverse order.

Thermodynamic Considerations. The rest of this Discussion will focus on the mechanism in Scheme 1. In terms of the thermodynamics of the reaction, is the description complete, or are there any steps missing that have a large free energy change? We can approach this by considering the overall equilibrium constant for the NF1-catalyzed hydrolysis and see if the rate and equilibrium constants that were determined for individual steps are consistent with this overall equilibrium constant. An example of a system where an extra step was required, and indeed important for the biological function, is given by the actomyosin ATPase (*46*). An extra actomyosin·ADP state was shown on the basis of kinetic measurements and that this state could not be formed in significant amounts by mixing actomyosin with ADP. Rather, it was formed transiently during ATP hydrolysis, following P_i release. Consideration of these different ADP

states was important for understanding the biochemical basis for force generation by different product states.

The equilibrium constant for GTP hydrolysis at approximately the conditions used here (low ionic strength, 30 °C, pH 7.5, saturating Mg^{2+}) can be calculated as $[GDP][P_i]/[GTP] = 2.2 \times 10^5$ M from figures in Alberty and Goldberg (*47*) for ATP, which are likely to apply closely to GTP also. Note that this calculation uses the convention that reactant water concentration is dimensionless and that the product H^+ is removed from the equilibrium equation by multiplying the "true" equilibrium constant by the proton concentration ($10^{-7.5}$ M).

The equilibrium constant for hydrolysis of Ras-bound nucleotides ([Ras·GDP][P_i]/[Ras·GTP]) can then be calculated, since the relative affinities of GDP and GTP for Ras are known, albeit at 37 °C. The relative affinity is represented by [Ras·GTP][GDP]/[Ras·GDP][GTP], and the equilibrium constant is 12 (*43*).

The equilibrium constant for the NF1-mediated hydrolysis is also [Ras·GDP][P_i]/[Ras·GTP], as the Ras starts and finishes dissociated from the NF1. This equilibrium constant is ([GDP][P_i]/[GTP])/([Ras·GTP][GDP]/[Ras·GDP][GTP]), i.e., $(2.2 \times 10^5 \text{ M})/12 = 1.8 \times 10^4$ M.

In terms of Schemes 1 and 2, this equilibrium constant is given by $K_{1a}k_{+1b}k_{+2}k_{+3}K_4/k_{-1b}k_{-2}k_{-3}$ Using the values in Table 3 and the value of K_4 found previously, this equilibrium constant is ~3500, 5-fold less than the value calculated above. However, several of the individual parameters may be out by factors of up to 2. The oxygen exchange data allows such a factor for k_{-2}. The relative affinities of GDP and GTP for Ras were measured at 37 °C rather than 30 °C. Some measurements in this work were done with natural nucleotides some with mant nucleotides and small differences in rate constants may be due to this. The rate of NF1 dissociation was measured using Ras·mantGMPPNP, rather than GTP to circumvent problems due to hydrolysis.

Thus, we can conclude that there is no need to include extra steps in Scheme 1 purely on the basis of thermodynamics. Scheme 1 and the rate constants found are a full description of the hydrolysis in these terms.

Active to Inactive Transition. Scheme 1 must be a simplification, as it is known that a major conformation change occurs during the conversion from the Ras·GTP state to the Ras·GDP state. The above analysis suggests that this conformation change is likely to occur during one of the steps defined in Scheme 1. Step 1 probably represents two processes (binding and some conformation change) on the basis of the measurement of binding kinetics, as in Scheme 2a. Which other steps might include processes such as conformation changes? The hydrolysis step is likely to be a single process, as it has been shown that for Ras alone the reaction occurs via an in-line displacement of GDP by water (*48*). This is likely to hold in the presence of NF1 also, on the basis of structural considerations (*8*, *9*). At present there seems no need to implicate further conformation changes in this step with NF1 (*49*).

The simplest interpretation would be that the NF1·Ras·GDP·P_i state maintains the Ras in the "GTP-like" conformation and the switch to the "GDP-like" conformation occurs during subsequent dissociation. A possible clue to the stage when this occurs is the slow rate of P_i binding, 108 M^{-1} s^{-1}, which is several orders of magnitude less than that expected for a diffusion-controlled process.

This anomaly might be resolved in two ways by dividing step 3 (P_i release) into two steps. First, the rate constant determination for P_i binding assumed that all Ras·GDP is available for binding P_i. As described above for actomyosin, this may not be the case. As shown in Scheme 2b and considered in the reverse (P_i binding) direction, there could be a conformation change of NF1·Ras·GDP, resulting in a very small concentration of NF1·Ras·GDP′. This can then bind P_i rapidly; however, because its concentration is small, the effective, overall rate constants for step 3 would remain as in Table 3. As an example, we could choose $k_{+3a} = 8$ s^{-1} (observed by P_i sensor), $k_{-3a} = 1.1 \times 10^6$ $M^{-1}s^{-1}$, and $k_{+3b}/k_{-3b} = 10^4$. Limits can be put on this model because simulations show that unless k_{+3b} is large ($>10^4$), addition of millimolar P_i would be expected to inhibit the GTPase activity. This is not observed.

An alternative division of step 3 into two is to have a conformation change occurring in the NF1·Ras·GDP·P_i (Scheme 2c). Again, considering the scheme in the reverse direction, P_i binds rapidly but this is followed by a conformation change that results in the overall rate constants for step 3 as in Table 3. Two examples of rate constants can be postulated in order to predict P_i binding at ~10^6 M^{-1} s^{-1}. In the first case, the conformation change is rate-limiting for P_i release: $k_{+3a} = 8$ s^{-1}, $k_{-3b} = 1.1 \times 10^6$ M^{-1} s^{-1}, and $k_{+3b}/k_{-3a} = 10^4$. The observed rate of P_i release would be limited by the rate of the conformation change, step 2a. In this case no inhibition by P_i would be observed, and this is fully consistent with the data so far. In the second case, the conformation change is rapid followed by slow P_i release: $k_{+3b} = 8$ s^{-1}, $k_{-3b} = 1.1 \times 10^6$ M^{-1} s^{-1}, and $k_{+3a}/k_{-3a} = 10^4$. This predicts a very low K_d for P_i, so that addition of P_i to the medium should have a large effect on NF1 binding to Ras·GDP·P_i should also inhibit the GTPase activity. Neither of these effects of P_i is observed, so this model can be excluded.

Another possibility is that step 4 is subdivided (Scheme 2d), so that two Ras·GDP states exist, but only one is able to bind NF1 effectively. However, this model is not consistent with the observed K_4 of 38 μM without imposing a very fast rate constant on NF1 binding, faster than likely limitations of diffusion control. A final possibility to get a true rate constant of P_i binding close to diffusion control is to consider if the form of P_i that binds is present as only a fraction of the total P_i. The obvious possibility is that only one protonated form binds (and by implication is released). But this model would require that active form to be present at ~0.1% of the total, to give a rate constant for P_i binding close to diffusion limited. To be present in a very small fraction, this active form of P_i would need to be H_3PO_4 or PO_4^{3-}, neither of which are attractive candidates to be the bound form, even transiently. So this possibility is readily dismissed.

Thus, to accommodate the slow P_i binding, either extension of the model (Scheme 2a or b) is consistent with the data, although there is no direct evidence for such an extra division of a step. It is then possible to postulate that the conformation change introduced might be the transition from the GTP-like (active) to GDP-like (inactive) state of Ras. The

NF1·Ras·GDP·P_i state formed by step 2 is in the GTP-like state. There is then a slow P_i release followed by rapid conformation change to the GDP state. In this model, P_i release might be considered as triggering the change in conformation to the inactive state of Ras. This in turn has a low affinity for NF1, which dissociates rapidly.

Alternatively, the NF1·Ras·GDP·P_i state formed on cleavage undergoes a slow (8 s^{-1}) conformation change, followed by rapid P_i release. In this model, it might be considered that the cleavage step 2 triggers the formation of the inactive state and the latter then triggers P_i release. In either case the key transition from active to inactive Ras states is closely linked with P_i release.

In conclusion, we have measured most rate constants in the GTPase reaction mechanism of Ras activated by the GTPase activating protein, NF1. In doing so we have shown that the slowest biochemical process is P_i release, severalfold slower than the preceding hydrolysis step. The changes in mant fluorescence monitor NF1 association to and dissociation from Ras. The NF1 dissociation is probably rapid and follows a Ras conformation change accompanying P_i release. This conformation change is likely to be that from the "GTP" structure to the "GDP" structure observed in crystal structures.

REFERENCES

1. Brunger, A. T., Milburn, M. V., Tong, L., de Vos, A. M., Jancarik, J., Yamaizumi, Z., Nishimura, S., Ohtsuka, E., and Kim, S. H. (1990) Crystal structure of an active form of RAS protein, a complex of a GTP analogue and the HRAS p21 catalytic domain, *Proc. Natl. Acad. Sci. U.S.A. 87*, 4849−4853.
2. Kim, S. H., de Vos, A. M., Tong, L., Miburn, M. V., Matias, P. M., Jancarik, J., Ohtsuka, E., and Nishimura, S. (1988) Ras oncogene proteins: three-dimensional structures, functional implications, and a model for signal transducer, *Cold Spring Harbor Symp. Quant. Biol. 53*, 273−281.
3. Pai, E. F., Kabsch, W., Krengel, U., Holmes, K. C., John, J., and Wittinghofer, A. (1989) Structure of the guanine-nucleotide-binding domain of the Ha-ras oncogene product p21 in the triphosphate conformation, *Nature 341*, 209−214.
4. Gideon, P., John, J., Frech, M., Lautwein, A., Clark, R., Scheffler, J. E., and Wittinghofer, A. (1992) Mutational and kinetic analyses of the GTPase-activating protein (GAP)-p21 interaction: the C-terminal domain of GAP is not sufficient for full activity, *Mol. Cell. Biol. 12*, 2050−2056.
5. Trahey, M., and McCormick, F. (1987) A cytoplasmic protein stimulates normal N-ras p21 GTPase, but does not affect oncogenic mutants, *Science 238*, 542−545.
6. Vogel, U. S., Dixon, R. A., Schaber, M. D., Diehl, R. E., Marshall, M. S., Scolnick, E. M., Sigal, I. S., and Gibbs, J. B. (1988) Cloning of bovine GAP and its interaction with oncogenic ras p21, *Nature 335*, 90−93.
7. Xu, G., O'Connell, P., Viskochil, D., Cawthon, R., Robertson, M., Culver, M., Dunn, D., Stevens, J., Gesteland, R., White, R., and Weiss, R. (1990) The neurofibromatosis type 1 gene encodes a protein related to GAP, *Cell 62*, 599−608.
8. Scheffzek, K., Ahmadian, M. R., Kabsch, W., Wiesmuller, L., Lautwein, A., Schmitz, F., and Wittinghofer, A. (1997) The ras-rasGAP complex: structural basis for GTPase activation and its loss in oncogenic ras mutants, *Science 277*, 333−338.
9. Ahmadian, M. R., Stege, P., Scheffzek, K., and Wittinghofer, A. (1997) Confirmation of the arginine-finger hypothesis for the GAP-stimulated GTP-hydrolysis reaction of Ras, *Nat. Struct. Biol. 4*, 686−690.
10. Martin, G. A., Viskochil, D., Bollag, G., McCabe, P. C., Crosier, W. J., Haubruck, H., Conroy, L., Clark, R., O'Connell, P., Cawthon, R. M., Innis, M. A., and McCormick, F. (1990) The GAP-related domain of the neurofibromatosis type 1 gene product interacts with ras p21, *Cell 63*, 843−849.
11. Tong, L., Milburn, M. V., de Vos, A. M., and Kim, S. H. (1989) Structure of ras proteins, *Science 245*, 244.
12. Schlichting, I., Almo, S. C., Rapp, G., Wilson, K., Petratos, K., Lentfer, A., Wittinghofer, A., Kabsch, W., Pai, E. F., Petsko, G. A., and Goody, R. S. (1990) Time-resolved X-ray crystallographic study of the conformational change in Ha-ras p21 protein on GTP hydrolysis, *Nature 345*, 309−315.
13. Schaber, M. D., Garsky, V. M., Boylan, D., Hill, W. S., Scolnick, E. M., Marshall, M. S., Sigal, I. S., and Gibbs, J. B. (1989) Ras interaction with the GTPase-activating protein (GAP), *Proteins: Struct., Funct., Genet. 6*, 306−315.
14. Brownbridge, G. G., Lowe, P. N., Moore, K. J. M., Skinner, R. H., and Webb, M. R. (1993) Interaction of GTPase activating proteins (GAPs) with p21ras measured by a novel fluorescence anisotropy method. Essential role of Arg-903 of GAP in activation of GTP hydrolysis on p21ras, *J. Biol. Chem. 268*, 10914−10919.
15. Eccleston, J. F., Moore, K. J. M., Morgan, L., Skinner, R. H., and Lowe, P. N. (1993) Kinetics of interaction between normal and proline 12 ras and the GTPase-activating proteins p120-GAP and neurofibromin, *J. Biol. Chem. 268*, 27012−27019.
16. Ahmadian, M. R., Hoffmann, U., Goody, R. S., and Wittinghofer, A. (1997) Individual rate constants for the interaction of ras proteins with GTPase-activating proteins determined by fluorescence spectroscopy, *Biochemistry 36*, 4535−4541.
17. Nixon, A. E., Brune, M., Lowe, P. N., and Webb, M. R. (1995) Kinetics of inorganic phosphate release during the interaction of p21ras with the GTPase activating proteins, p120-GAP and neurofibromin, *Biochemistry 34*, 15592−15598.
18. Sermon, B. A., Lowe, P. N., Strom, M., and Eccleston, J. F. (1998) The importance of two conserved arginine residies for catalysis by the ras GTPase-activating protein, neurofibromin, *J. Biol. Chem. 273*, 9480−9485.
19. Allin, C., Ahmadian, M. R., Wittinghofer, A., and Gerwert, K. (2001) Monitoring the GAP catalyzed H−Ras GTPase reaction at atomic resolution in real time, *Proc. Natl. Acad. Sci. U.S.A. 98*, 7754−7759.
20. Webb, M. R., and Trentham, D. R. (1981) The mechanism of ATP hydrolysis catalyzed by myosin and actomyosin, using rapid reaction techniques to study oxygen exchange, *J. Biol. Chem. 256*, 10910−10916.
21. Shukla, K. K., and Levy, H. M. (1977) Mechanism of oxygen exchange in actin-activated hydrolysis of adenosine triphosphate by myosin subfragment 1, *Biochemistry 16*, 132−135.
22. Levy, H. M., and Koshland, D. E. (1959) *J. Biol. Chem. 234*, 1102−1107.
23. Boyer, P. D. (1989) A perspective of the binding change mechanism for ATP synthesis, *Faseb. J. 3*, 2164−2178.
24. Hackney, D. D., and Boyer, P. D. (1978) Subunit interaction during catalysis. Implications of concentration dependency of oxygen exchanges accompanying oxidative phosphorylation for alternating site cooperativity, *J. Biol. Chem. 253*, 3164−3170.
25. Hibberd, M. G., Webb, M. R., Goldman, Y. E., and Trentham, D. R. (1985) Oxygen exchange between phosphate and water accompanies calcium-regulated ATPase activity of skinned fibers from rabbit skeletal muscle, *J. Biol. Chem. 260*, 3496−3501.
26. Bowater, R., Zimmerman, R. W., and Webb, M. R. (1990) Kinetics of ATP and inorganic phosphate release during hydrolysis of ATP by skeletal actomyosin subfragment 1: oxygen exchange between water and ATP or phosphate, *J. Biol. Chem. 265*, 171−176.
27. Webb, M. R., Hibberd, M. G., and Goldman, Y. E. (1986) Phosphate-water oxygen exchange probe of Ca2+-activation of isometric chemically skinned fibers from rabbit skeletal muscle, *Biophys. J. 49*, 448a.
28. Neal, S. E., Eccleston, J. F., and Webb, M. R. (1990) Hydrolysis of GTP by $p21^{N-ras}$, the *NRAS* protooncogene product, is accompanied by a conformational change in the wild-type protein: use of a single fluorescent probe at the catalytic site, *Proc. Natl. Acad. Sci. U.S.A. 87*, 3562−3565.
29. Scheidig, A. J., Franken, S. M., Corrie, J. E. T., Reid, G. P., Wittinghofer, A., Pai, E. F., and Goody, R. S. (1995) X-ray crystal structure analysis of the cata lytic domain of the oncogene product p21H-ras complexed with caged GTP and Mant dGppNHp, *J. Mol. Biol. 253*, 132−150.
30. Hall, A., and Self, A. J. (1986) The effect of Mg^{2+} on the guanine nucleotide exchange rate of p21N-ras, *J. Biol. Chem. 261*, 10963−10965.
31. Skinner, R. H., Bradley, S., Brown, A. L., Johnson, N. J. E., Rhodes, S., Stammers, D. K., and Lowe, P. N. (1991) Use of the Glu-Glu-Phe C-terminal epitope for rapid purification of the catalytic domain of normal and mutant ras GTPase-activating proteins, *J. Biol. Chem. 266*, 14163−14166.

32. Marchuk, D. A., Saulino, A. M., Tavakkol, R., Swaroop, M., Wallace, M. R., Andersen, L. B., Mitchell, A. L., Gutmann, D. H., Boguski, M., and Collins, F. S. (1991) cDNA cloning of the type 1 neurofibromatosis gene: complete sequence of the NF1 gene product, *Genomics 11*, 931−940.
33. Brune, M., Hunter, J. L., Howell, S. A., Martin, S. R., Hazlett, T. L., Corrie, J. E. T., and Webb, M. R. (1998) Mechanism of inorganic phosphate interaction with phosphate binding protein from *Escherichia coli*, *Biochemistry 37*, 10370−10380.
34. Hiratsuka, T. (1983) New ribose-modified fluorescent analogues of adenine and guanine nucleotides available as substrates for various enzymes, *Biochim. Biophys. Acta 742*, 496−508.
35. Jameson, D. M., and Eccleston, J. F. (1997) Fluorescent nucleotide analogues: synthesis and applications, *Methods Enzymol. 278*, 363−390.
36. Newcombe, A. R., Stockley, R. W., Hunter, J. L., and Webb, M. R. (1999) The interaction between rac1 and its guanine nucleotide dissociation inhibitor (GDI), monitored by a single fluorescent coumarin attached to GDI, *Biochemistry 38*, 6879−6886.
37. Hirshberg, M., Stockley, R. W., Dodson, G., and Webb, M. R. (1997) The crystal structure of human rac1, a member of the rho-family complexed with a GTP analogue, *Nat, Struct. Biol. 4*, 147−152.
38. Wang, J. H., Xiao, D. G., Deng, H., Callender, R., and Webb, M. R. (1998) Vibrational study of phosphate modes in GDP and GTP and their interaction with magnesium in aqueous solution, *Biospectroscopy 4*, 219−227.
39. Webb, M. R., Hibberd, M. G., Goldman, Y. E., and Trentham, D. R. (1986) Oxygen exchange between water and medium P_i during ATP hydrolysis mediated by skinned fibers from rabbit skeletal muscle: evidence for P_i binding to a force-generating state, *J. Biol. Chem. 261*, 15557−15564.
40. Eccleston, J. F., Hutchinson, J. P., and White, H. D. (2001) Stopped-flow techniques, in *Protein Ligand Interactions: Structure and Spectroscopy. A Practical Approach Series* (Harding, S. E., and Chowdry, B. Z., Eds.) pp 201−237, Oxford University Press, Oxford.
41. Leatherbarrow, R. J. (2001) *Grafit Version 5*, Erithacus Software Ltd., Horley, U.K.
42. Brune, M., Hunter, J. L., Haire, L. F., Henrick, K., Hirshberg, M., Corrie, J. E. T., and Webb, M. R. (1998) Mechanism of phosphate binding to the phosphate binding protein of *E. Coli* using coumarin-labeled protein and the crystal structure of the labeled protein, *Biophys. J. 74*, A64, *Biophys. J. 74*, A64.
43. Neal, S. E., Eccleston, J. F., Hall, A., and Webb, M. R. (1988) Kinetic analysis of the hydrolysis of GTP by p21N-ras: the basal GTPase mechanism, *J. Biol. Chem. 263*, 19718−19722.
44. Webb, M. R. (1992) *The role of nucleoside triphosphate hydrolysis in transducing systems: p21ras and muscle*, *Philos. Trans. R. Soc. London, Ser. B 336*, 19−24.
45. Shutes, A., Phillips, R. A., Corrie, J. E. T., and Webb, M. R. (2002) The role of magnesium in nucleotide exchange on the small G protein rac, investigated using novel fluorescent guanine nucleotide analogues, *Biochemistry 41*, 3828−3835.
46. Sleep, J. A., and Hutton, R. L. (1980) Exchange between inorganic phosphate and adenosine 5′-triphosphate in the medium by actomyosin subfragment 1, *Biochemistry 19*, 1276−1283.
47. Alberty, R. A., and Goldberg, R. N. (1992) Standard thermodynamic formation properties for the adenosine 5′-triphosphate series, *Biochemistry 31*, 10610−10615.
48. Feuerstein, J., Goody, R. S., and Webb, M. R. (1989) The mechanism of guanosine nucleotide hydrolysis by p21c-Ha-ras: the stereochemical course of the GTPase reaction, *J. Biol. Chem. 264*, 6188−6190.
49. Rensland, H., Lautwein, A., Wittinghofer, A., and Goody, R. S. (1991) Is there a rate-limiting step before GTP-cleavage by H-ras p21, *Biochemistry 30*, 11181−11185.

BI027316Z